Guided magneto-plasmon polaritons in thin films: non-reciprocal propagation and forbidden modes

2008 J. Phys.: Condens. Matter 20 335217

(http://iopscience.iop.org/0953-8984/20/33/335217)

IOP Publishing Journal of Physics: Condensed Matter

J. Phys.: Condens. Matter **20** (2008) 335217 (8pp) doi:10.1088/0953-8984/20/33/335217

Guided magneto-plasmon polaritons in thin films: non-reciprocal propagation and forbidden modes

B L Johnson and Hsiao-Harng Shiau

Department of Physics and Astronomy, Western Washington University, Bellingham, WA 98225-9164, USA

Received 16 April 2008, in final form 7 July 2008
Published 28 July 2008
Online at stacks.iop.org/JPhysCM/20/335217

Abstract

We study the dispersion and electric field distributions of magneto-plasmon polaritons propagating in thin films of conductors separated by a thin insulating dielectric film. The system supports guided modes, which exist at frequencies and wavenumbers generally forbidden; the coupled surface plasmon polaritons of the system exhibit propagation which is non-reciprocal with the application of a transverse DC magnetic field. The forbidden guided modes are symmetric with respect to propagation direction, and therefore the combinations of effects offer interesting device application possibilities.

1. Introduction

The study of plasmons in coupled systems, thin films and superlattices has been a subject of great interest for many years [1–7]. Recently, advances in nanofabrication and processing of metal and semiconductor materials has lead to renewed interest in plasmons, plasmon polaritons (PPs) and other related collective charge and spin excitations. In particular, there has been interest in signal transmission, routing and coupling [8, 9]. In addition, there has been considerable work investigating the properties of polariton waveguide principles and device applications, including the enhancement of light transmission through metal films with nanostructured apertures [10], manipulation of optical couplers via surface PPs on microstructured wire arrays [11], and other thin film and photonic bandgap devices [12, 13]. The existence of guided-wave polariton modes has also been established for thin metal films [14] and active control mechanisms for coupling low-frequency PPs on semiconductors have been proposed [15], as well as other important effects including negative refraction [16–18], nonlinear (harmonic generation) effects [19, 20] and plasmonic solutions [21].

In this paper, we will focus on the fundamental properties of PPs on thin films of conducting material coupled by thin dielectric films, under a transverse DC magnetic field; the system supports an interesting array of PP modes, including collective surface modes and guided-wave modes [22]. Collective-mode PPs on layered structures provide the opportunity to tailor the dispersion properties of the excitations; studies of collective modes on superlattices have produced many interesting results [1]. The main idea is that plasmon polaritons localized at the boundary between a conductor and an insulator produce fields which extend into the dielectric and which can couple to an adjacent conducting surface. For an array of thin films, the surface waves thus couple to produce collective modes of the whole structure, the properties of which depend upon the overall geometry and intrinsic material properties of the structure.

The addition of a transverse DC magnetic field can have significant impact on the properties of PP modes [1]. The field gives rise to a 'handedness' for the plasma oscillations of the conductor, thereby lowering the symmetry of the overall structure. In particular, surface waves in coupled systems can become non-reciprocal [23]—the propagation frequency for modes with wavevector $\vec{k}$ can differ from that of modes with wavevector $-\vec{k}$. Therefore, for device applications, modes traveling in opposite directions become decoupled, and signals of a given wavelength can pass in opposite directions independently. In this paper, we investigate the non-reciprocal behavior of surface PPs, as well as the effects of transverse magnetic fields on the forbidden guided-wave PP modes.

The two-film/dielectric system studied here supports a wide array of 'forbidden' guided PP modes, depending upon the geometry and material properties (i.e. the overall symmetry) of the constituent films [16]. Ordinary PP collective modes are composed of coupled waves localized at each conductor/insulator interface; in contrast, the forbidden modes are composed of waves largely in the interior dielectric

between the conducting films. The dispersion of these guided modes forms a 'ladder' of allowed modes, always within a region of the dispersion space 'left' of the light line on graphs of frequency versus wavevector, i.e. for $ck < \omega$.

The main result of the current work is that, while the collective surface-wave PPs become highly non-reciprocal with applied DC magnetic field, the forbidden guided modes remain symmetrical with respect to propagation direction. The non-reciprocal propagation of the *surface* PPs depends strongly on the structural symmetry of the system; a simple symmetry argument provides a clue to this behavior: for a given configuration of propagation vector, structure geometry and magnetic field, if a set of symmetry operations can take $\vec{k}$ to $-\vec{k}$ and leave the rest of the system unchanged, then the propagation must be reciprocal. If the operations leave the system in a different configuration, then the propagation may be non-reciprocal. Since the guided-wave modes have a different character from the pure surface-constructed modes—they are not composed of coupled surface waves that exist on the individual film surfaces and thus do not exist when the films are widely separated—the argument does not apply.

The main result has important device application possibilities, as signal processing may be accomplished via the surface-wave PPs as well as the guided-wave modes. It has been shown that couplers and/or surface-wave probes (such as ATR) can be used to drive and detect the PP modes; the possibilities proposed here are rich, since the application of the magnetic field can decouple (in frequency) surface waves traveling in opposite directions, while at the same time leaving the guided-wave modes unchanged; in addition, the application of even modest magnetic fields can change the localization of coupled surface waves, and thus give rise to possible switching mechanisms.

The rest of this paper is organized as follows. In section 2 we outline the theory for modeling PPs in a thin-film system. In section 3 we present numerical studies of the PP dispersion and electric field distributions for a variety of model structures, and in section 4 we present a brief summary of the main results.

2. Theory

In this section, we present an outline of the theoretical methods for calculating allowed plasmon polariton excitations in a coupled thin-film system. We consider the geometry depicted in figure 1; the system consists of two conducting films (films labeled 2 and 4 in the figure), separated by an insulating spacer, with the bottom conductor resting on a semi-infinite substrate. The system is considered infinite in the x–z plane, and regions of different material are numbered accordingly. The thicknesses and dielectric constants of regions indexed by integer n are given by d_n and ε_n, respectively. In the interest of completeness, we will initially assume that all dielectric constants are frequency-dependent.

The first step in finding the collective-mode dispersion relation for the structure of figure 1 is to solve the electromagnetic wave equation appropriate to each region, and match the solutions across regions using the appropriate boundary conditions. For brevity, we will focus on p-polarized

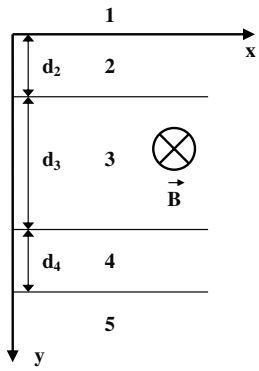

Figure 1. The geometry considered in this paper. The different layers of material are labeled, along with their thickness. The conducting layers are labeled 2 and 4.

plasmon polariton modes. We first write the general wave equation (with $\mu = 1$ everywhere)

$$\nabla \times \nabla \times \vec{E} = -\frac{1}{c^2}\frac{\partial^2 \vec{D}}{\partial t^2}. \tag{2.1}$$

In the absence of a magnetic field, solving the wave equation would be a matter of assuming plane-wave-like solutions in each region, $e^{i(\vec{k}\cdot\vec{r}-\omega t)}$ (where $\vec{k}$ and ω are the polariton propagation vector and frequency, respectively), and given linear isotropic media, the constitutive relation $\vec{D} = \overleftrightarrow{\varepsilon}\vec{E}$ would immediately give a simple two-component wave equation in terms of the electric field vector alone (two-component because we note that $\vec{k}\cdot\hat{z} = 0$ for p-polarized modes). With the application of a static magnetic field along the z axis in figure 1, the constitutive relation is more complex. In this case, the dielectric tensor appropriate for region n is given by

$$\varepsilon_n = \begin{bmatrix} \varepsilon_{na} & -i\varepsilon_{nb} \\ i\varepsilon_{nb} & \varepsilon_{na} \end{bmatrix} \tag{2.2}$$

where the components are, explicitly,

$$\begin{aligned} \varepsilon_{na} &= \varepsilon_{\infty n}\left(1 + \frac{\omega_{pn}^2}{\omega_{cn}^2 - \omega^2}\right) \\ \varepsilon_{nb} &= \varepsilon_{\infty n}\left(\frac{\omega_{cn}\omega_{pn}^2}{\omega\left(\omega_{cn}^2 - \omega^2\right)}\right) \end{aligned} \tag{2.3}$$

and, for region n, $\varepsilon_{\infty n}$ is the background dielectric constant, ω_{pn} is the plasma frequency and $\omega_{cn} = eB/m_n^* c$ is the cyclotron frequency, with B the magnetic field strength and m_n^* the appropriate effective mass. We have assumed negligible damping. In this case, we can write the wave equations (2.1) appropriate to each region as

$$\begin{bmatrix} \omega_0^2\varepsilon_{na} - k_{ny}^2 & i\omega_0^2\varepsilon_{nb} + k_x k_{ny} \\ -i\omega_0^2\varepsilon_{nb} + k_x k_{ny} & \omega_0^2\varepsilon_{na} - k_x^2 \end{bmatrix} \begin{bmatrix} E_{nx} \\ E_{ny} \end{bmatrix} = 0 \tag{2.4}$$

where $\omega_0 = \omega/c$, and we note that the parallel component of the wavevector k_x is conserved, and is therefore the same in each layer and does not require an index. In order

that (2.4) yield linearly independent solutions, the determinant of the coefficient matrix must vanish, so that the wavevector components are related by

$$k_{ny}^2 = \omega_0^2 \left(\varepsilon_{na} - \frac{\varepsilon_{nb}^2}{\varepsilon_{na}} \right) - k_x^2. \tag{2.5}$$

Equations (2.4) and (2.5) may now be combined, so that the field amplitudes in the two axes can be related to one another; the point is to utilize the continuity of the component of the electric field parallel to the interfaces to write the general electric field in a useful manner. Equations (2.4) and (2.5) yield the relation

$$E_{ny} = -\left(\frac{\varepsilon_{na} k_x^2 + (\omega_0 \varepsilon_{nb})^2}{\varepsilon_{na} \left(k_x k_{ny} - \mathrm{i}\omega_0^2 \varepsilon_{nb} \right)} \right) E_{nx}. \tag{2.6}$$

The general solution for the electric field vector in a given region can be written as a superposition of waves traveling in the $+y$ and $-y$ directions; taking advantage of equation (2.6), and denoting the tangential amplitudes of the plus and minus traveling waves as A_n and B_n, respectively, we have

$$E_n = \begin{bmatrix} \hat{x} \\ -\alpha_n^- \hat{y} \end{bmatrix} A_n \mathrm{e}^{\mathrm{i}(k_x x + k_{ny} y - \omega t)} + \begin{bmatrix} \hat{x} \\ \alpha_n^+ \hat{y} \end{bmatrix} B_n \mathrm{e}^{\mathrm{i}(k_x x - k_{ny} y - \omega t)}, \tag{2.7}$$

where

$$\alpha_n^{\mp} = \frac{\varepsilon_{na} k_x^2 + (\omega_0 \varepsilon_{nb})^2}{\varepsilon_{na} \left(k_x k_{ny} \mp \mathrm{i}\omega_0^2 \varepsilon_{nb} \right)} \tag{2.8}$$

comes from equations (2.6), with all k_{ny} taken to be positive. At this point, we can assemble the coupled system by matching the appropriate boundary conditions at each interface. Matching the tangential components of $\vec{E}$ and the normal components of $\vec{D}$ at each boundary yields the following matrix equation:

$$\begin{bmatrix} 1 & -1 & -1 & 0 & 0 \\ R_1 & -Q_2 & -R_2 & 0 & 0 \\ 0 & \mathrm{e}^{\mathrm{i}k_{2y}d_2} & e^{-\mathrm{i}k_{2y}d_2} & -1 & -1 \\ 0 & Q_2 \mathrm{e}^{\mathrm{i}k_{2y}d_2} & R_2 \mathrm{e}^{-\mathrm{i}k_{2y}d_2} & -Q_3 & -R_3 \\ 0 & 0 & 0 & \mathrm{e}^{\mathrm{i}k_{3y}d_3} & e^{-\mathrm{i}k_{3y}d_3} \\ 0 & 0 & 0 & Q_3 \mathrm{e}^{\mathrm{i}k_{3y}d_3} & R_3 \mathrm{e}^{-\mathrm{i}k_{3y}d_3} \\ 0 & 0 & 0 & 0 & 0 \\ 0 & 0 & 0 & 0 & 0 \end{bmatrix}$$
$$\begin{bmatrix} 0 & 0 & 0 \\ 0 & 0 & 0 \\ 0 & 0 & 0 \\ 0 & 0 & 0 \\ -1 & -1 & 0 \\ -Q_4 & -R_4 & 0 \\ \mathrm{e}^{\mathrm{i}k_{4y}d_4} & e^{-\mathrm{i}k_{4y}d_4} & -1 \\ Q_4 \mathrm{e}^{\mathrm{i}k_{4y}d_4} & R_4 \mathrm{e}^{-\mathrm{i}k_{4y}d_4} & -Q_5 \end{bmatrix} \begin{bmatrix} B_1 \\ A_2 \\ B_2 \\ A_3 \\ B_3 \\ A_4 \\ B_4 \\ A_5 \end{bmatrix} = 0, \tag{2.9}$$

where $Q_n = \mathrm{i}\varepsilon_{nb} - \alpha_n^- \varepsilon_{na}$ and $R_n = \mathrm{i}\varepsilon_{nb} + \alpha_n^+ \varepsilon_{na}$. Given the system of equations (2.9), the PP dispersion relations can be calculated by choosing a value for k_x, and then solving for the value of ω which causes the determinant of the coefficient matrix in (2.9) to vanish. Furthermore, the tangential components of the electric field amplitudes are computed by inserting the appropriate values for $\vec{k}$ and ω, and solving (2.9) for the amplitudes A_n in terms of the first amplitude B_1.

In the next section, we will solve the system of equations (2.9) numerically for a variety of situations.

3. Numerical examples

In this section, we perform and analyze numerical studies of the formalism introduced in the previous section. The geometry in all cases is assumed to be that depicted in figure 1, with the magnetic field into the plane of the figure; the two free-charge layers (layer 2 and layer 4) are assumed to be doped GaAs films separated by and surrounded by insulating dielectrics. The dielectric function for the GaAs layers is given by equations (2.3), with a static-limit dielectric constant of $\varepsilon_\infty = 13.13$. The film thicknesses are given by $t_2 = t_4 = t = 0.57c/\omega_p$ and $t_3 = 5t$. The main goal of this section will be to demonstrate the effects of the magnetic fields on the plasmon polariton spectrum, and the material parameters will be chosen to best represent the major effects. In what follows all units will be scaled: unitless frequency is given by $\Omega = \omega/\omega_p$ and unitless wavevector by $K_\parallel = ck_x/\omega_p$. The purpose of the scaling is to render the results general; the plasma frequency depends on the actual doping levels of the active layers (as well as the signs of the free carriers), and possibilities range across the infrared, assuming typical carrier densities from 10^{17} to 10^{20} cm^{-3}. Therefore, by controlling doping levels, the systems described in this section can be accessible to appropriate sources and detectors.

Some general features of PPs are as follows: in all cases presented here, the PP modes break roughly into two types, characterized by the vertical component of the wavevector, k_y. For pure real k_y, the solutions are wavelike inside a given layer, while for pure imaginary k_y, the modes in a given layer are surface waves which decay exponentially into the material. The condition for surface polaritons in a given region is given by equation (2.5), i.e. $k_x^2 > \varepsilon(\omega/c)^2$, or, for conducting (doped) layers, $\omega < \sqrt{c^2 k_x^2/\varepsilon_\infty + \omega_p^2}$ and for insulating layers, $\omega < ck_x/\varepsilon$. These relations mark the boundaries of the 'bulk modes' and the 'light line,' respectively, within a given material.

In figure 2, we show the dispersion relations for a system with perfect reflection symmetry about the midplane: here the spaces above, below, and between the two GaAs layers are assumed to be vacuum ($\varepsilon = 1$). For completeness, we show both positive and negative values of $K_\parallel$, even though the high-symmetry forces the dispersion to be reciprocal. Note the bulk-mode boundaries and light line denoted by dashed lines in the figure. The solid lines to the right of the light lines are the allowed surface-constructed PP modes, and the mode penetrating into the 'forbidden' region is a guided-wave mode—the field amplitudes for all of these modes will be discussed below. It is important to note that, due to the midplane-reflection symmetry, the dispersion curves depicted in figure 2 do not change with applied magnetic field (as mentioned above); the dispersion shown is reciprocal with respect to propagation direction and the level frequencies do

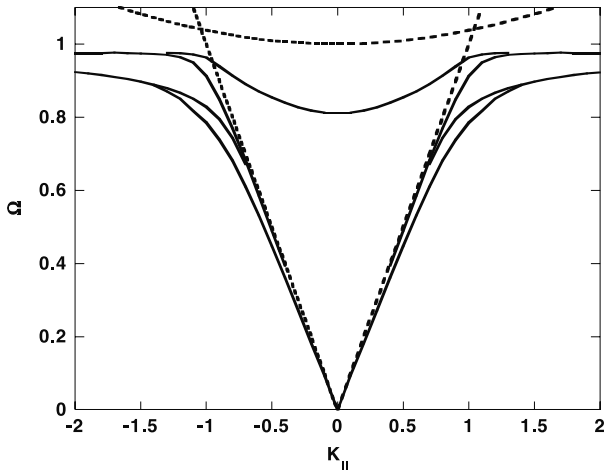

Figure 2. The dispersion curve frequency versus wavenumber (in reduced units) for the symmetric case given by two GaAs conducting layers separated and surrounded by vacuum. The dotted lines are the bulk-mode boundary and the vacuum light line. Note that this curve is the same for zero magnetic field and for small applied fields, and that the modes are reciprocal with respect to propagation direction.

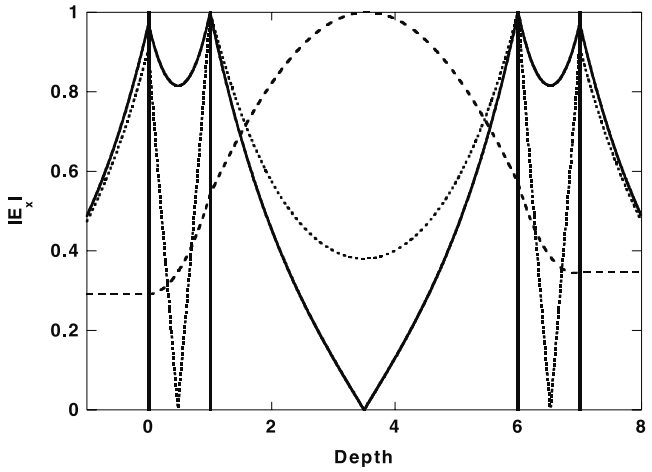

Figure 3. The electric field amplitudes as a function of depth into the structure for selected plasmon polariton modes from figure 2, with no applied magnetic field. The layer boundaries are included for clarity. The modes here are given by the ordered pair $(K_\parallel, \Omega)$ as follows: (1.5, 0.892) solid curve; (1.5, 0.977) dotted curve; (0.5, 0.854) for the dashed curve. Note the reflection symmetry about the structure midplane.

not shift much under modest magnetic field. The electric field *amplitudes*, however, do respond to modest applied fields.

In figure 3, we show the magnitude of the tangential electric field components (arbitrary units) as a function of depth into the structure (in units of t) for three different polariton modes at zero magnetic field. The boundaries of the different layers have been included in the figure as a guide to the eye. The solid and dotted curves represent surface-constructed modes, with $K_\parallel = 1.5$ and $\Omega = 0.892$, $\Omega = 0.977$ for each, respectively; these modes are found on the branches of the dispersion to the right (in wavevector) of the light line, and thus obey the relationship demanded above of surface waves. Note that, for each of these modes, the electric fields are localized to the boundary surfaces and decay exponentially into the material. The dashed curve is for the forbidden guided mode, with $K_\parallel = 0.5$ and $\Omega = 0.854$, which is also constructed of surface waves, but which takes the form of a 'standing' wave resulting from the coupling of the two active layers. In the large-t_3 limit (i.e. $t_3 \to \infty$), the system reverts to two uncoupled single-film structures, where the guided-wave mode does not exist, and the other surface modes merge and converge to the single-film polariton dispersion. The guided-wave mode arises as one of the high-frequency single-film surface modes and is a result purely of the coupling between the films. The coupling splits the single-film modes, and the high-energy surface mode pair produces the GWM. (For a discussion of the details of isolated structures versus the distance dependence of the coupled electromagnetic modes of layered structures, see [24].) Note the overall symmetry of all modes, mimicking the reflection symmetry of the structure, both in terms of the geometric and the electromagnetic symmetry; note that the phase information for the waves is lost when taking the absolute magnitude, so the odd–even symmetries are also lost (hard zeros represent π phase shifts). For instance, the solid curves represent an odd-symmetry mode about the midplane.

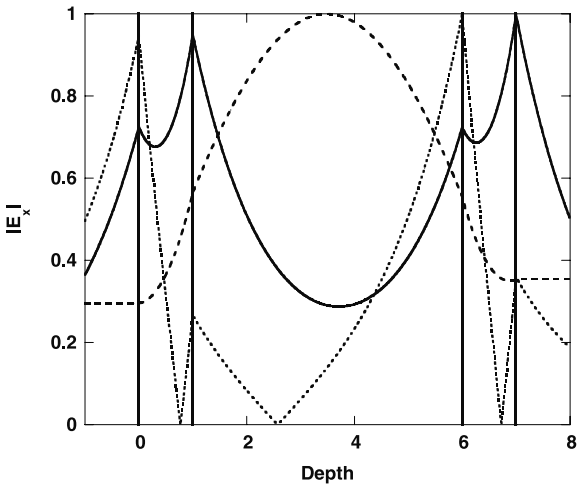

Figure 4. The electric field amplitudes for the same modes as those in figure 3, except here the magnetic field is given by $\Omega_c = 0.05$. Note that the surface-constructed modes are localized more strongly on the bottom conductor, while the guided-wave mode (dashed curve) remains peaked at the midplane.

In contrast, figure 4 shows the same modes as those in figure 3, but with an applied parallel magnetic field given by $\Omega_c = \omega_c/\omega_p = 0.05$. Here there is no appreciable shift in the dispersion relations, but the lowering of the electromagnetic symmetry starts to localize the surface modes. Note that the solid curve and the dotted curve begin to show localization towards the bottom, with the solid curve localized at the bottom surface while the dotted curve is localized on the inner boundary of the bottom GaAs layer. Remarkably, however, there is almost no change at all for the field amplitudes of the guided-wave mode (dashed curve). This is a major feature of the current system; the symmetry lowering effects of the magnetic field do not appreciably affect the guided modes, due

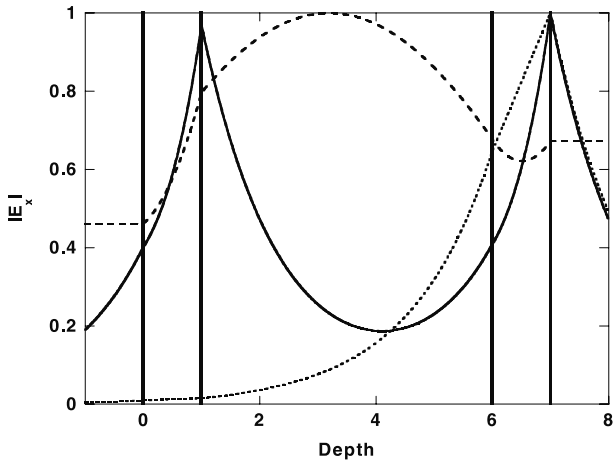

Figure 5. The electric field amplitudes for the same modes as figure 3, under a magnetic field given by $\Omega_c = 0.5$. Note the strong localization of the surface-constructed modes and the relative insensitivity of the guided-wave mode.

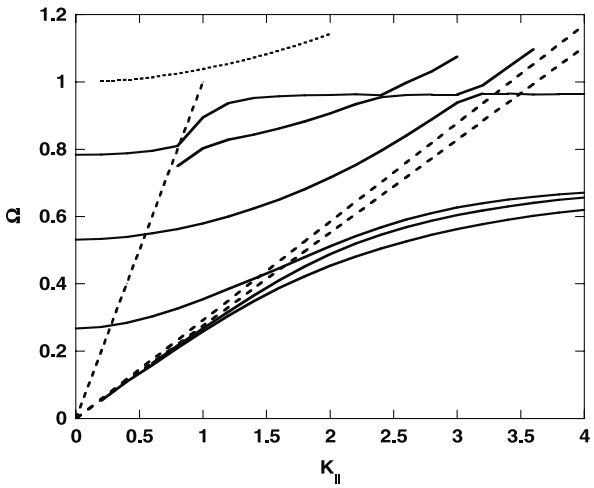

Figure 6. The zero magnetic field dispersion curves for the model system given by two doped layers of GaAs, separated by an Si layer, resting on an undoped GaAs substrate. Once again, the dashed and dotted lines are the light line and bulk-mode boundary, respectively. Note the ladder of guided-wave modes that exists inside the vacuum light line, as explained in the text.

to the change in character of the GWM from pure surface-constructed to bulk-like.

In figure 5, the same modes as those in figure 4 are shown, but this time at a higher magnetic field: $\Omega_c = 0.5$. In this case, the dispersion has shifted slightly with respect to the zero-field case (but the entire dispersion remains reciprocal with respect to $K_\parallel \rightarrow -K_\parallel$); for the solid curve $K_\parallel = 1.5, \Omega = 0.723$, for the dotted curve $K_\parallel = 1.5, \Omega = 0.842$ and for the dashed curve $K_\parallel = 0.5, \Omega = 0.826$. Note that the applied field has localized the higher-energy mode completely to the bottom surface; the lower-energy surface mode is still localized on the bottom surface but also still has appreciable amplitude and symmetry. The guided mode is shifted slightly towards the bottom surface; however, the peak amplitude remains at the midpoint of the gap separating the doped layers.

The more interesting cases involve the lowering of the structure symmetry prior to the application of the magnetic field; in this way, there is no reflection symmetry about the midplane, and therefore the symmetry operations that take $K_\parallel \rightarrow -K_\parallel$ involve operations that do not leave the system (including applied magnetic field) unchanged. In figure 6 we show the zero magnetic field dispersion curves for the case $\varepsilon_1 = 1, \varepsilon_3 = 11.7, \varepsilon_5 = 13.13$. These are the values appropriate for a trial system consisting of doped GaAs on an insulating GaAs substrate, separated from another doped layer by a layer of silicon, with vacuum above. As mentioned in previous work [22], this system represents a physically realizable system that is ideal for creating a 'ladder' of guided-wave modes; the large substrate dielectric has a light line well away from that of vacuum, and thus pulls the long-wavelength (small wavevector) surface polaritons away for the vacuum light line, creating a large parameter space for the guided-wave modes to propagate [22]. In figure 6, we see the three light lines, one for vacuum, one for Si and one for GaAs, as well as the ladder of three distinct guided-wave modes. The zero magnetic field system is reciprocal with respect to $K_\parallel$, so only one side of the dispersion is shown. Because the dielectric layers have three different dielectric constants, this

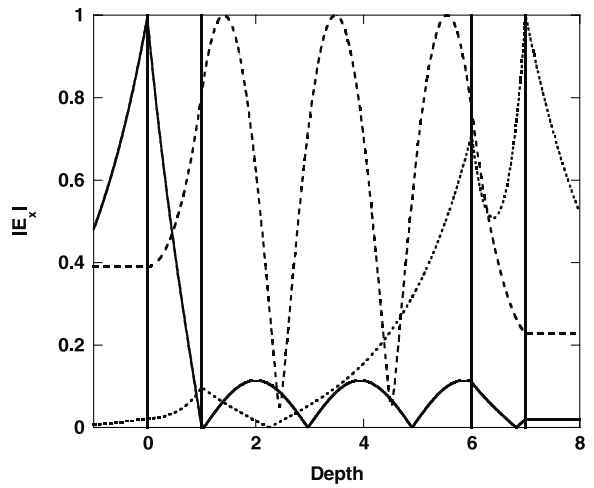

Figure 7. Electric field amplitudes for selected modes from figure 6. The modes are given by (1.6, 0.957) solid curve; (2.0, 0.453) dotted curve; (0.4, 0.788) dashed curve. Note the surface-constructed modes are localized by the lower dielectric symmetry.

system represents the lowest possible structural symmetry, and we expect the magnetic field to produce highly non-reciprocal surface polaritons. In addition, we note that the guided-wave modes evolve out of the bulk-mode edge, and from the highest-energy surface mode. The evolution is interesting, in that the modes undergo several anti-crossings as a function of wavevector.

For the zero-field case of figure 6, we expect that the low electromagnetic symmetry will compel each surface-constructed polariton mode to be localized to a different surface. In figure 7, we show the electric field amplitudes for modes from different regions of the dispersion curves. The solid line is for the mode at $K_\parallel = 1.6, \Omega = 0.957$, inside the semiconductor light lines and inside of the anti-crossing

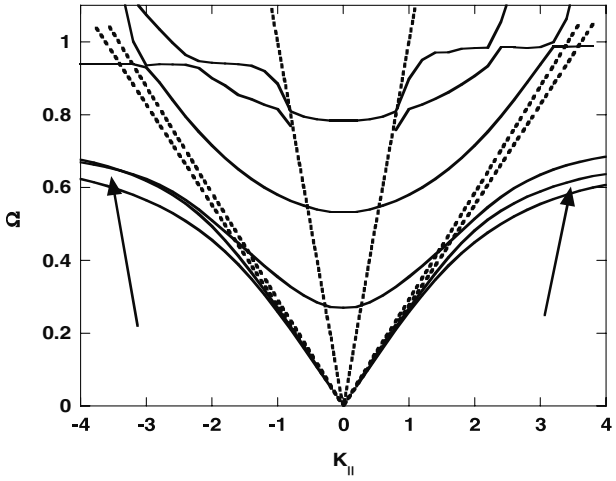

Figure 8. The dispersion curves for the GaAs–Si system of figure 6, under a small applied field given by $\Omega_c = 0.05$. Note the non-reciprocal (different allowed frequency for change in wavevector sign) modes indicated by the arrows. The guided-wave modes remain reciprocal with respect to propagation direction.

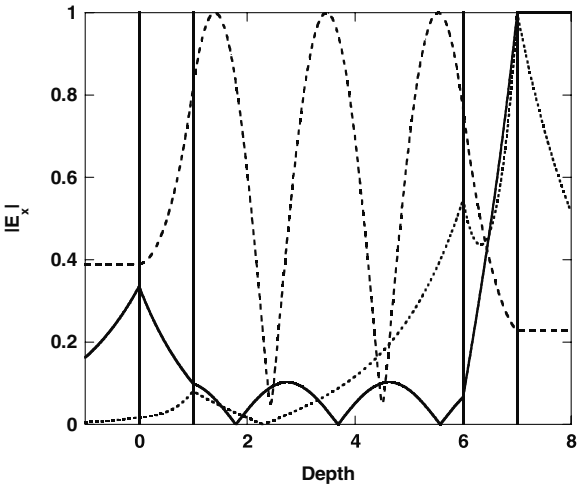

Figure 9. The electric field amplitudes corresponding to the same modes as those in figure 7, but with the small applied magnetic field $\Omega_c = 0.05$. Note that the mode previously localized at the upper boundary surface (solid curve) is now localized to the lower boundary surface.

in the highest-energy surface-constructed mode. Note that this mode is entirely localized at the top interface, bounding the top active GaAs layer with the vacuum. This is the character of the mode throughout, starting from the region $K_\parallel > 3.5$. The dotted mode is given by $K_\parallel = 2.0, \Omega = 0.453$, which is the uppermost of the triplet of modes to the right of the semiconductor light lines—it is also the mode that evolves into the low-energy guided-wave mode in the forbidden region. Note that this mode is localized to the bottom boundary, between the bottom active GaAs layer and the Ga As substrate. The dashed mode is the highest-energy guided-wave mode in the forbidden region left of the vacuum light line, at $K_\parallel = 0.4, \Omega = 0.788$. Here the number order of the mode (in frequency) coincides with the number of peaks that exist in the Si gap; this mode has three peaks, etc.

We now turn to the effect of applied magnetic field to the low-symmetry structure. Figure 8 shows the dispersion curves appropriate to the Si–GaAs system, for both signs of $K_\parallel$, under a small applied magnetic field given by $\Omega_c = 0.05$. Even with the modest applied field, the surface-constructed PP modes are highly non-reciprocal: note the splitting of the triplet of low-energy surface waves, depicted by the arrows in the figure; however, it is very interesting to note that the energies of the guided-wave modes are *not* sensitive to the applied field and remain reciprocal. This is due to the different mode character, i.e. the bulk-like nature of the GWM, and thus the electromagnetic symmetry arguments for the surface waves do not apply.

In figure 9, we track the changes in the electric field amplitudes for the same modes as those in figure 7, but now the effect of the small magnetic field is studied. The solid curve, given by $K_\parallel = 1.6, \Omega = 0.971$, has reversed its localization, and now, remarkably, is localized to the bottom surface. This behavior is the result of modes changing character after an anti-crossing: Note that in figure 6 the horizontal high-frequency surface mode passes through several anti-crossings

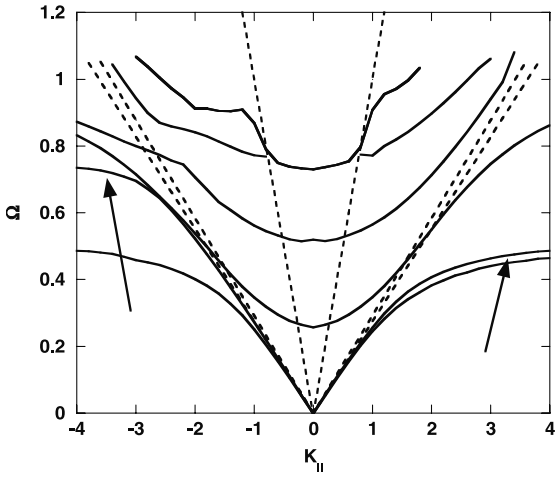

Figure 10. The dispersion curves for the GaAs–Si system of figure 6, but under a magnetic field given by $\Omega_c = 0.5$. Note the pronounced non-reciprocity for the surface waves indicated by the arrows, while the guided-wave ladder remains reciprocal.

(the splitting caused by the coupling of the layers requires the anti-crossings, see [22]); the actual mode changes, but the character of the mode does not. With the applied magnetic field, the character inversion can occur as the anti-crossing is shifted. The reversion behavior may have important device applications, as detecting the mode by surface-sensitive means such as attenuated total reflection will show a switching effect with the application of small magnetic field for this (constant-frequency) mode. The dotted curve, now given by $K_\parallel = 2.0, \Omega = 0.449$, is relatively insensitive to the small applied field, as is the guided-wave mode—the dashed curve in the figure with $K_\parallel = 0.4, \Omega = 0.788$ (exactly the same dispersion frequency as the zero-field mode).

In figure 10, the dispersion for the same Si–GaAs system under a higher field, given by $\Omega_c = 0.5$, is shown. The

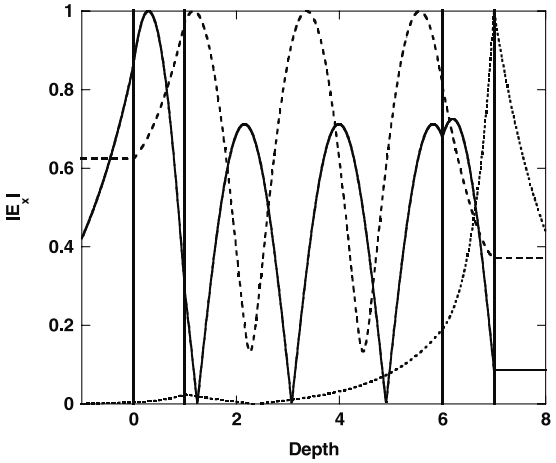

Figure 11. The electric field amplitudes for the GaAs–Si structure under a magnetic field of $\Omega_c = 0.5$. The single surface-constructed mode is strongly localized (dotted curve), while the other surface mode has changed character to bulk-like behavior (solid curve). Again, the guided-wave mode (dashed curve) is not sensitive to the magnetic field.

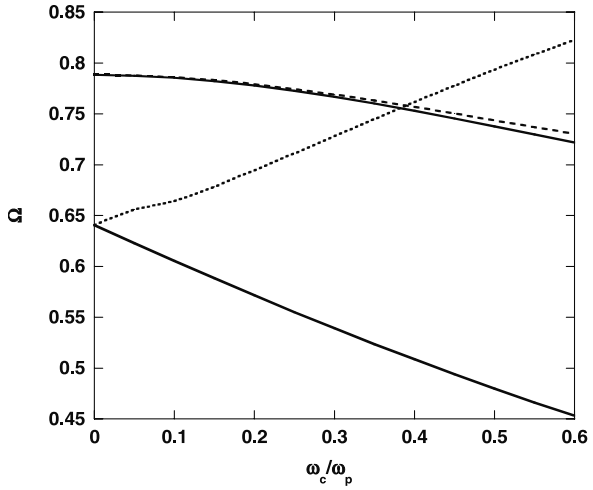

Figure 12. A plot of allowed frequency versus applied magnetic field (reduced units) for modes at fixed $\pm K_\parallel$. For the modes starting at high frequency (corresponding to guided-wave modes), the curves are for $K_\parallel = \pm 0.4$ solid and dashed, respectively, while for the lower-frequency (surface) modes $K_\parallel = \pm 3.6$ dotted and solid curves, respectively. Note the marked non-reciprocity for the surface modes, and the relative insensitivity for the guided-wave modes.

major features to note here are the very strong non-reciprocal behavior of the middle surface-constructed mode (shown by arrows) and the now pronounced downward shift in frequency for the three guided-wave modes—which are *still reciprocal* with respect to propagation direction. The uppermost mode (in frequency) between the vacuum and semiconductor light lines is also highly non-reciprocal, and has changed its character considerably.

To see the character change in what was, with no applied magnetic field, a top-surface localized mode, we show again the same three electric field distributions for the high-field case in figure 11. The solid curve, with $K_\parallel = 1.6, \Omega = 0.996$, is clearly evolving into bulk-mode behavior—it has been shifted such that, although it still has solutions applicable for the surface mode states discussed above, its character is that of a bulk mode, localized inside the active layer. In contrast, the dotted curve, with $K_\parallel = 2.0, \Omega = 0.383$, remains relatively insensitive to the magnetic field and is still localized entirely to the bottom surface of the bottom active layer. Perhaps most remarkably, the guided-wave mode ($K_\parallel = 0.4, \Omega = 0.744$) still remains almost entirely unchanged; the guided modes remain reciprocal and their electric field distribution is independent of the applied field.

From the point of view of device physics, the structure described here has remarkable possibilities; the non-reciprocal surface waves provide the basis for signal process in which signals propagating on the structure in opposite directions have different frequencies, the basis for a directional switch. Moreover, the guided-wave modes, which are reciprocal and whose localization character is unaffected by the magnetic field, provide a 'baseline' signal processing mode and, as mentioned above, the fact that the upper-surface mode undergoes a dramatic 'switching' effect with the application of very small magnetic fields represents another basic signal processing application.

To illustrate the magnitude of the non-reciprocal behavior as a function of applied magnetic field, figure 12 shows the allowed frequencies at different wavevectors, plotted as a function of Ω_c. The upper lines are for $K_\parallel = \pm 0.4$, solid and dashed, respectively, while the lower-frequency curves are for $K_\parallel = \pm 3.6$, dotted and solid lines, respectively. The figure illustrates the dramatic non-reciprocity of the surface-constructed modes (lower curves) and the relative insensitivity of the guided-wave modes (upper curves) as a function of applied field.

4. Summary

In this paper, we have derived the dispersion and electric field amplitudes for plasmon polaritons propagating on coupled thin-film structures under a magnetic field applied parallel to the film interfaces. The primary purpose of the paper is to illustrate the effect of an applied DC magnetic field on the surface-constructed plasmon polariton modes as well as on the interesting modes that exist in the parameter space forbidden to single-mode (uncoupled) surface polariton waves. We find that the coupled surface-constructed polariton modes are highly non-reciprocal with respect to propagation direction, but that the guided-wave modes are almost entirely insensitive to applied field. In addition, the surface-constructed modes localized at the top surface of the bi-layer structure switch character, and are localized to the bottom surface with the application of very small magnetic fields. All of these effects have potentially important signal processing device applications.

Acknowledgment

This work was supported by the NSF, under grant no. DMR0705908.

References

[1] Johnson B L and Camley R E 1991 *Phys. Rev.* B **43** 6554
[2] Guiliani G F and Quinn J J 1983 *Phys. Rev. Lett.* **51** 919
[3] Olego D, Pinzuk A, Gossard A C and Wiegmann W 1982 *Phys. Rev.* B **25** 7867
[4] Sood A K, Mendez J, Cardona M and Ploog K 1985 *Phys. Rev. Lett.* **54** 2115
[5] Haupt R and Wendler L 1987 *Phys. Status Solidi* b **142** 423
[6] Farias G A, Auto M M and Albuquerque E L 1988 *Phys. Rev.* B **38** 12540
[7] Albuquerque E L and Cottam M G 2004 *Polaritons in Periodic and Quasiperiodic Structures* (Amsterdam: Elsevier)
[8] Berini P 2001 *Phys. Rev.* B **63** 125417
[9] Novikov I V and Maradudin A A 2002 *Phys. Rev.* B **66** 035403
[10] Barnes W L, Murray W A, Dintinger J, Devaux E and Ebbesen T W 2004 *Phys. Rev. Lett.* **92** 107401
[11] Christ A, Tikhodeev S G, Gippius N A, Kuhl J and Giessen H 2003 *Phys. Rev. Lett.* **91** 183901
[12] Bozhevolnyi S I 2001 *Phys. Rev. Lett.* **86** 3008
[13] Ditlbacher H, Krenn J R, Dereux A, Lamprecht B, Lacroute Y and Goudonnet J P 2002 *Appl. Phys. Lett.* **81** 1762
[14] Charbonneau R, Bernini P, Berolo E and Lisicka-Shrzek E 2000 *Opt. Lett.* **25** 844
[15] Gomez Rivas J, Kuttge M, Kurz H, Haring Bolivar P and Sanchez-Gil J A 2006 *Appl. Phys. Lett.* **88** 082106
[16] Wood B, Pendry J B and Tsai D P 2006 *Phys. Rev.* B **74** 115116
[17] Fan X B, Wang G P, Lee J C-W and Chan C T 2006 *Phys. Rev. Lett.* **97** 073901
[18] Scadora M *et al* 2007 *Opt. Express* **15** 508
[19] Bennink R S, Yoon Y K and Boyd R W 1999 *Opt. Lett.* **24** 1416
[20] Lepeshkin N N, Schweinsberg A, Piredda G, Bennink R S and Boyd R W 2004 *Phys. Rev. Lett.* **93** 123902
[21] Liu Y, Bartal G, Genov D and Zhang X 2007 *Phys. Rev. Lett.* **99** 153901
[22] Gilmore M A and Johnson B L 2003 *J. Appl. Phys.* **93** 4497
[23] Johnson B L and Camley R E 1988 *Phys. Rev.* B **38** 3311
[24] Gilmore M A and Johnson B L 2001 *Eur. Phys. J.* B **23** 297